$K^*(890)$ Production in the Charge Exchange Reaction $K^+n \to K^+\pi^-p$ at 9 GeV/c.†

D. Cords, D. D. Carmony, H. W. Clopp, A. F. Garfinkel

R. F. Holland, F. J. Loeffler, H. B. Mathis and L. K. Rangan

Purdue University, Lafayette, Indiana 47907

J. Erwin, R. L. Lander, D. E. Pellett and P. M. Yager

University of California, Davis, California 95616

W. L. Yen and F. T. Meiere

Indiana University-Purdue University, Indianapolis, Indiana 46205

(Received)

The dominant production mechanism for the reaction $K^+n \to pK^*(890)$ is π-exchange and the energy dependence of the cross section is found to be proportional to $P_{lab}^{-2.2}$. The conventional absorption model does not reproduce the rapid decrease of ρ_{00} as a function of the four momentum transfer. The Reggeized π-A_2 model of Dass and Froggatt reproduces the t-dependence of ρ_{00} and Re ρ_{10} but there is serious disagreement for ρ_{1-1} which may indicate the need to include A_1 exchange. The asymmetry in the decay angular distribution is interpreted as S-P wave interference.

1. Introduction

In this article we present results from our analysis of the charge exchange reaction

$$K^+n \to K^+\pi^-p \qquad (1)$$

at 9 GeV/c. We obtained 3882 events of this type from approximately 280,000 pictures, taken at the Brookhaven 80" deuterium filled bubble chamber exposed in an r.f.

DISCLAIMER

separated beam. This corresponds to a microbarn equivalent of 8 events/μb.

The most dominantly produced meson resonances are the $K^*(890)$ and $K^*(1420)$, as can be seen in Fig. 1a. The $K\pi$ mass distribution in Fig. 1a was fitted with a superposition of two Breit-Wigner distributions and a smooth, hand-drawn background, achieving a confidence level of 84%. The fit gave masses of 893 ± 2 and 1416 ± 6 MeV, widths of 53 ± 7 and 144 ± 22 MeV, and cross sections of 61 ± 9 and 66 ± 10μb for the $K^*(890)$ and $K^*(1420)$ respectively. The cross sections contain a 5% correction due to the Glauber screening and the Pauli principle, but no corrections for unseen decay modes. Fig. 1b shows the $p\pi^-$ mass distribution (unshaded for all events). From the shaded $p\pi$ mass distribution in Fig. 1b ($M_{K\pi} < 1.5$ GeV) it seems likely that baryon resonances, if present, constitute only a small background under the K^* peaks.

2. $K^*(890)$ Production in Charge Exchange Reactions

The production mechanism of $K^*(890)$ can be studied by investigating the energy dependence of the charge exchange reactions

$$K^+n \to K^{*o}(890)p \qquad (2)$$

$$K^-p \to K^{*o}(890)n \qquad (3)$$

and by analyzing their decay angular distributions.

2.1 Energy Dependence

We have compared the predictions of the absorption model[1,2] with the $K^*(890)$ data. The absorption model predictions were calculated within the formalism given by Jackson and collaborators[1,2] using basically their prescription for selecting the parameters.[3] The absorption parameters vary with the type of reaction and with energy. Figs. 1c and 1d show the differential cross sections for the 3 GeV/c CERN data[4b] of reaction (2) and our data at 9 GeV/c for the same reaction. Events with a $K\pi$ mass between 0.84 and 0.94 GeV have been selected. Not only the shape of the t-distributions is reproduced correctly, but also the change in the cross section by an order of magnitude is accounted for. The energy dependence of both charge exchange reactions (2) and (3) is further illustrated in Fig. 1f, where we present

a compilation[4,5] of cross sections for various incident momenta (uncorrected for unseen decay modes). The full circles stand for reaction (2) and the open circles for reaction (3). The full and dotted curves are the absorption corrected π-exchange calculations for reactions (2) and (3) respectively. Since the total cross section is higher for K^-p than for K^+n collisions, the absorption effect is stronger for reaction (3), and consequently the predictions for reaction (3) in Fig. 1f (dotted line) lie below the predictions for reaction (2) (solid line). However, for incident momenta above 5 GeV this effect is of the order of or smaller than the errors in the experimental cross sections. We observe a rough agreement between the experimental data and the model calculations. This agreement leads us to conclude that π-exchange is the main characteristic of the production mechanism for reactions (2) and (3).

The decrease of the absorption model predicted cross section with increasing incident momentum is slower than P_{lab}^{-2}, expected for unmodified π-exchange. The data points show, on the contrary, a somewhat faster decrease than P_{lab}^{-2}, and consequently support a Reggeized parameterization for π-exchange. Since there is no apparent distinction in the behavior of reactions (2) and (3), we fitted all experimental cross sections in Fig. 1f with the function $\sigma = A\left(\frac{P_{lab}}{P_o}\right)^{-n}$ where P_o = 1 GeV/c. Assuming 15% experimental errors in all cases the fit gave A = 9.2 ± 0.8 mb and n = 2.24 ± 0.15 with a confidence level of 46% (see dash-dotted line in Fig. 1f). The observation, that the cross sections for reactions (2) and (3) are equal within the present experimental errors, excludes any major contribution for odd C-parity exchanges, like ρ-exchange, in a model independent way.

2.2 Production Density Matrix

For the $K^*(890)$ with spin-parity 1^- the decay angular distribution is determined by the production density matrix. The density matrix elements have been calculated in the Jackson frame using the method of moments. Events were taken having a $K\pi$ effective mass between 0.84 and 0.94 GeV. In Fig. 2 the density matrix

elements are presented as a function of the momentum transfer squared $-t$ and compared to the absorption model calculations, discussed in the previous section (solid line). The experimental values for ρ_{00} decrease much faster than the absorption model prediction and show a peak rather than a dip for small momentum transfers. The agreement for Re ρ_{10} is fair, and again some disagreement is observed for ρ_{1-1} at $|t|$ values above 0.1 GeV^2.

In addition, these density matrix elements have been compared to the Reggeized π-exchange calculations of Dass and Froggatt[6] who include a small amount of A_2-exchange. The dotted and dash-dotted curves in Fig. 2 represent the evasive and conspiratorial solutions, respectively. The t-dependence of ρ_{00} is much better reproduced by these Regge model calculations than by the absorption model, and the agreement for Re ρ_{10} is comparable in both cases. Judging from the peaking of the experimental ρ_{00} distribution at small momentum transfers and from the zero-value of the experimental Re ρ_{10} point in the lowest bin, the evasive solution seems to be slightly preferred.[7] But such a distinction is far from being definite at the present stage of experimental accuracy.

There is a surprisingly large discrepancy for ρ_{1-1} between the Regge model calculations and the data, in particular for $|t|$ values above 0.2 GeV^2. The fact that the experimental values of ρ_{1-1} are compatible with zero over the t-range considered, implies that natural and unnatural parity exchange in addition to π-exchange have to occur in equal amounts.[8] Therefore, this discrepancy may give a hint that in addition to A_2-exchange some unnatural parity exchange with spin equal to or larger than 1 has to be included. A_1-exchange may be a suitable choice.[9] This point should be the subject of further investigation.

3. Interference Terms in the $K^*(890)$ Decay Correlations

After having discussed the production mechanism of the $K^*(890)$ one can turn to the detailed structure of the decay angular distribution. Both models discussed in the previous section predict a symmetric decay angular distribution. But this symmetry is not observed experimentally, as has been reported earlier.[4a, 4b]

In Fig. 3 we present the Jackson and Treiman-Yang angular distributions of the $K\pi$ system in reaction (1) for the $K^*(890)$ region and for two adjacent control regions. The distributions in the $K^*(890)$ region show a strong forward peaking in $\cos\theta_{K\pi}$ and a strong deviation from isotropy in $\phi_{K\pi}$. A tentative explanation of this behavior would be a double Regge mechanism consisting of Pomeron- and π-exchange as illustrated by the diagram in Fig. 1e. According to a conjecture of Harari,[10] this diagrem may provide a general type background for the $K\pi$ system. Calculations along this line, performed by Fu[11] for the reaction $K^+p \to K^+\pi^-\Delta^{++}(1236)$ at 9 GeV/c, show that a distinctive feature of this type of background is a forward peaking in the Jackson angle distribution and an anisotropic Treiman-Yang angle distribution.

Just these characteristics are observed in the $K^*(890)$ region. But to be sure about the origin of these effects one has to look at adjacent control regions as well. The lower region has only few events and the upper control region shows a backward peaking in $\cos\theta_{K\pi}$ and isotropy in $\phi_{K\pi}$, just the opposite expected from the double Regge exchange. One might still argue that constructive interference changes to destructive interference as the mass of the $K\pi$ system increases. But it is hard to see how the strong anisotropy in $\phi_{K\pi}$ should vanish at higher $K\pi$ masses, where the double Regge exchange is thought to become increasingly important. We therefore rule out the interference of $K^*(890)$ production with the double Regge mechanism as very unlikely.

In fact, the double Regge type background is probably negligible in the $K\pi$ mass range below 1.5 GeV. In Fig. 1b the $p\pi$ mass distribution for events with $M_{K\pi} \leq 1.5$ GeV is shown as the shaded histogram. No excessive low $p\pi$ mass enhancement, characteristic for double Regge exchange, is observed in the shaded histogram. This mechanism may be of some minor importance in the $K^*(1420)$ region and certainly dominates for $K\pi$ masses above 2 GeV.

In order to explain the asymmetry in the $K^*(890)$ decay angular distribution we turn to the traditional approach assuming an interference of the P-wave with an

S-wave background. We use a parameterization of this interference applied earlier to ρ^0 production in $\pi^- p \to \rho^0 n$[12] and $K^*(890)$ production in reaction (3)[5b]. In addition to the density matrix elements in the preceding section, Re ρ_{00}^{INT} and Re ρ_{10}^{INT} are introduced which represent the interference terms between S- and P-wave. Since Re ρ_{00}^{INT} is the coefficient of the cos θ term in the angular distribution, it accounts for the asymmetry in the Jackson angle distribution. Similarly, Re ρ_{10}^{INT} accounts for part of the anisotropy in $\phi_{K\pi}$. In Fig. 2 we present in addition to the density matrix elements, discussed in the previous section, the S-P wave interference density matrix elements. The interference terms are definitely different from zero in the $|t|$ range from 0 to 0.4 GeV^2.

We wish to thank the physicists and technicians at Brookhaven National Laboratory for their assistance during the exposure. We also thank Professor L. J. Gutay for helpful discussions, in particular for pointing out the implication of ρ_{1-1} being zero experimentally.

†Work supported in part by the U.S. Atomic Energy Commission.

1. K. Gottfried and J. D. Jackson, Nuovo Cimento 34, 735 (1964).

2. J. D. Jackson et al., Phys. Rev. 139, B428 (1965).
   J. T. Donohue, Phys. Rev. 163, 1549 (1967).

3. Because no data on K^+n elastic scattering are available the absorption parameters for reaction (2) were obtained from K^+p elastic scattering and the K^+n total cross section, compiled by: L. R. Price et al., UCRL-2000 K^+n (1969). The absorption parameters of reaction (3) were obtained from K^-p experimental data: V. S. Barashenkov, "Interaction Cross Section of Elementary Particles" (Moscow, 1966); L. S. Schroeder et al., Phys. Rev. 176, 1648 (1968). These data determine the absorption parameters in the initial state. There is some freedom as to the absorption parameters in the final state. A traditional choice has been $\gamma_f = \frac{3}{4}\gamma_i$ and $c_f = 1$ (see ref. 2). In our case we had to change this to $\gamma_f = \frac{1}{2}\gamma_i$, $c_f = 1$ in order to reproduce the steep decrease

of the t-distributions in Figs. 1c and 1d. The coupling constants are:

$$\frac{g^2_{K^{*o}K^+\pi^-}}{4\pi} = 1.5\ \text{GeV}^{-2}; \qquad \frac{g^2_{np\pi^-}}{4\pi} = 29.2\ \text{GeV}^{-2}\ .$$

4. a) S. Goldhaber et al., Phys. Rev. Letters 15, 737 (1965).
   b) G. Bassompierre et al., Nucl. Phys. B16, 125 (1970).
   c) A. Firestone et al., preprint UCRL-20076, (The quoted $K^*(890)$ cross section is our estimate from this preprint).
5. a) M. Dickenson et al., Phys. Letters 23, 505 (1966).
   b) M. Aguilar-Benitez et al., Phys. Rev. Letters 26, 466 (1971).
   c) F. Schweingruber et al., Phys. Rev. 166, 1317 (1968).
   d) Nijmegen-Amsterdam Collaboration, preprint (1971).
   e) M. Markytan, Nucl. Phys. B10, 193 (1969).
   f) B. D. Hyams et al., Nucl. Phys. B7, 1 (1968).
6. G. V. Dass and C. D. Froggatt, Nucl. Phys. B8, 661 (1968).
   G. V. Dass and C. D. Froggatt, Nucl. Phys. B10, 151 (1969).
7. The variation of t_{min} over the chosen $K^*(890)$ mass band is negligible with respect to the size of lowest -t bin in Fig. 2.
8. ρ_{11} represents the sum and ρ_{1-1} the difference of the natural and unnatural parity exchange contributions with spin equal to or larger than 1, see e.g.; R. H. Dalitz, Estratto da Rendiconti della Scuola Internazionale di Fisica, "E. Fermi", XXXIII Corso, p. 141 (1965).
9. B. Diu and M. LeBellac, Nuovo Cimento 53A, 158 (1968).
10. H. Harari, Phys. Rev. Letters 20, 1395 (1968).
11. C. Fu, Phys. Rev. D3, 92 (1971).
12. D. H. Miller et al., Phys. Review 153, 1423 (1967).

Figure Captions

Fig. 1: (a) $K^+\pi^-$ mass distribution fitted with a superposition of two Breit-Wigner distributions and a smooth hand-drawn background for masses below 1.66 GeV.

(b) $p\pi^-$ mass distribution for all events and, shaded, for events with $M_{K^+\pi^-} < 1.5$ GeV.

(c) and (d) $\frac{d\sigma}{dt}$ for $K^+n \to K^*(890)p$ for 3 and 9 GeV/c respectively. The curves are absolute predictions of the absorption model of Jackson et al.

(e) Double-Regge diagram including Pomeron and pion exchange.

(f) Total cross sections for reaction $K^+n \to K^*(890)p$ (full circles) at: 2.3 GeV/c (ref. 4a), 3.0 GeV/c (ref. 4b), 9.0 GeV/c (this expt.), 12.0 GeV/c (ref. 4c); and reaction $K^-p \to K^*(890)n$ (open circles) at: 2.0 GeV/c (ref. 5a), 3.9 GeV/c (ref. 5b), 4.1 GeV/c (ref. 5c), 4.2 GeV/c (ref. 5d), 4.6 GeV/c (ref. 5b), 5.5 GeV/c (ref. 5c), 10.0 GeV/c (ref. 5e), 11.2 GeV/c (ref. 5f). The full and dotted lines are the predictions of the absorption model for the first and second reaction respectively. The dash-dotted line is the fitted function $\sigma(P) = 9.2\left(\frac{P_{lab}}{P_o}\right)^{-2.24}$.

Fig. 2: Density matrix elements for $K^+n \to K^*(890)p$ at 9 GeV/c. The full curves are absorption model predictions of Jackson et al. The dotted and dash-dotted curves are Regge model predictions of Dass and Froggatt representing the evasive and conspirational solutions respectively. The S-wave interference, represented by Re ρ_{00}^{INT} and Re ρ_{10}^{INT}, is not taken into account by the model calculations.

Fig. 3: Jackson and Treiman-Yang angular distributions in the $K^*(890)$ region and in two control regions.

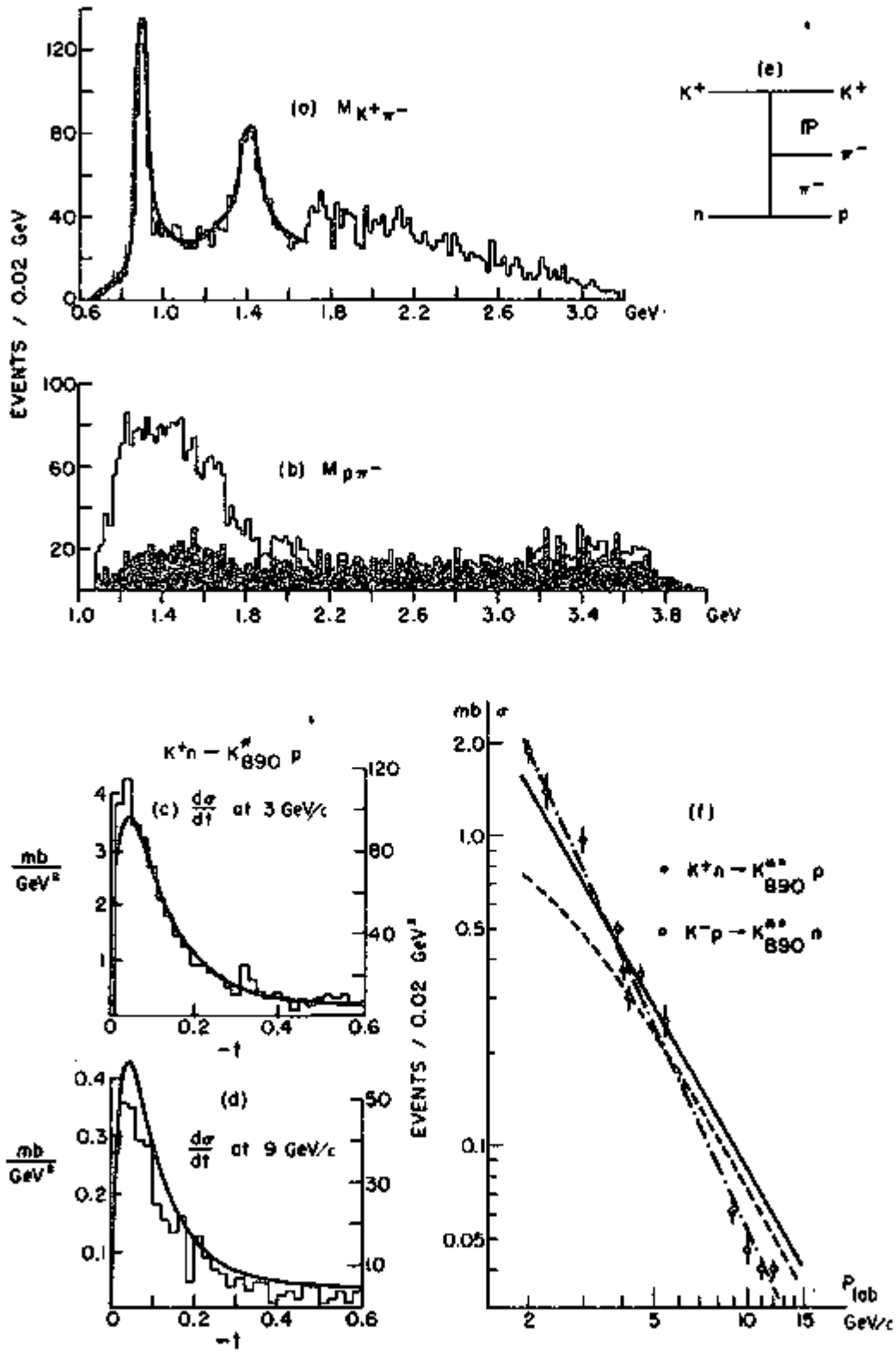
(a) $M_{K^+\pi^-}$
(b) $M_{p\pi^-}$
EVENTS / 0.02 GeV
GeV
(e)
K^+
K^+
IP
π^-
π^-
n
p
$K^+n \to K^{**}_{890}\,p$
(c) $\frac{d\sigma}{dt}$ at 3 GeV/c
(d) $\frac{d\sigma}{dt}$ at 9 GeV/c
$\frac{mb}{GeV^2}$
$-t$
mb
σ
(f)
$K^+n \to K^{**}_{890}\,p$
$K^-p \to K^{**}_{890}\,n$
EVENTS / 0.02 GeV^2
P_{lab}
GeV/c

FIG 1

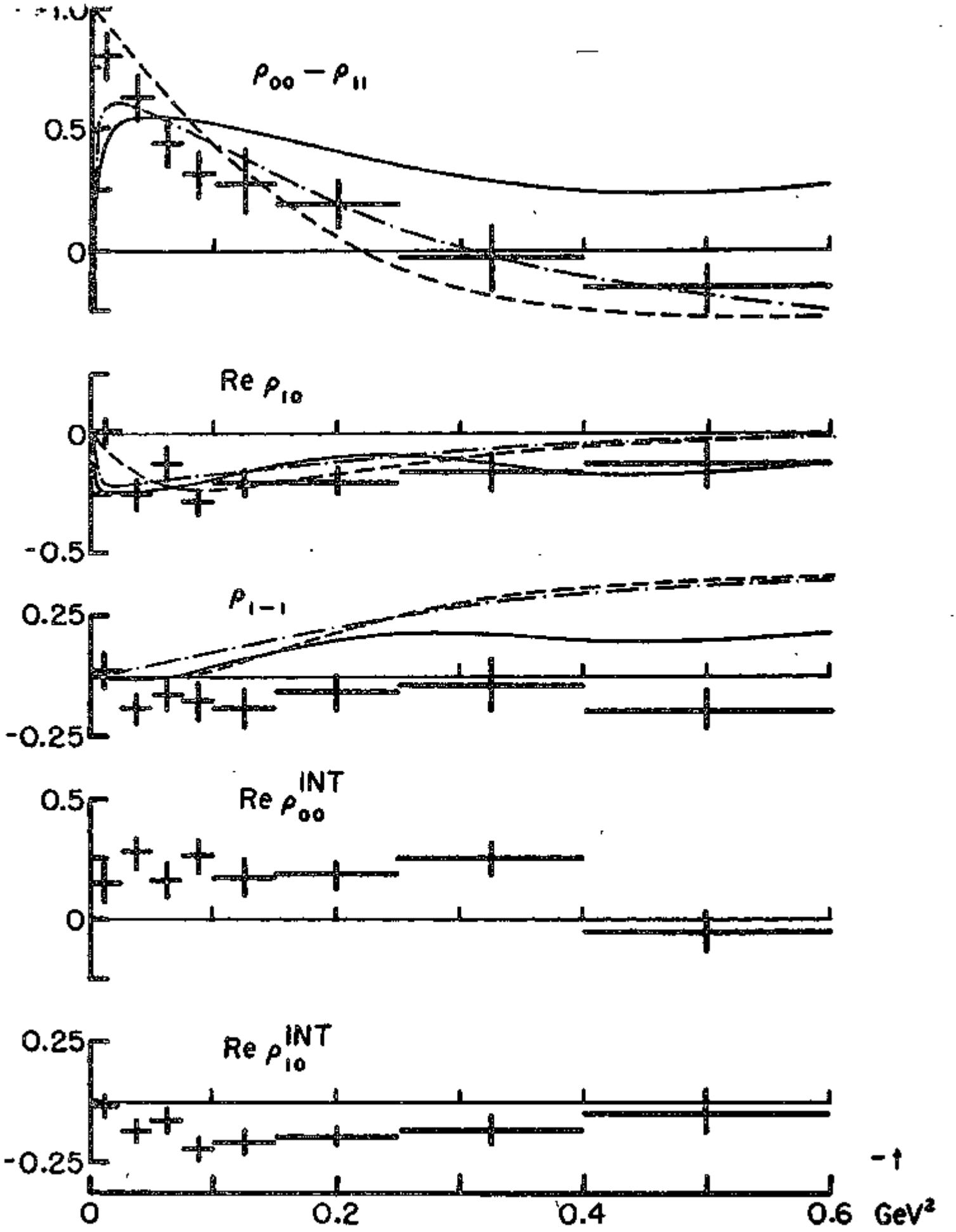
$\rho_{00} - \rho_{11}$
0.5
0
Re ρ_{10}
0
-0.5
ρ_{1-1}
0.25
-0.25
Re ρ_{00}^{INT}
0.5
0
Re ρ_{10}^{INT}
0.25
-0.25
$-t$
0
0.2
0.4
0.6 GeV²

FIG. 2

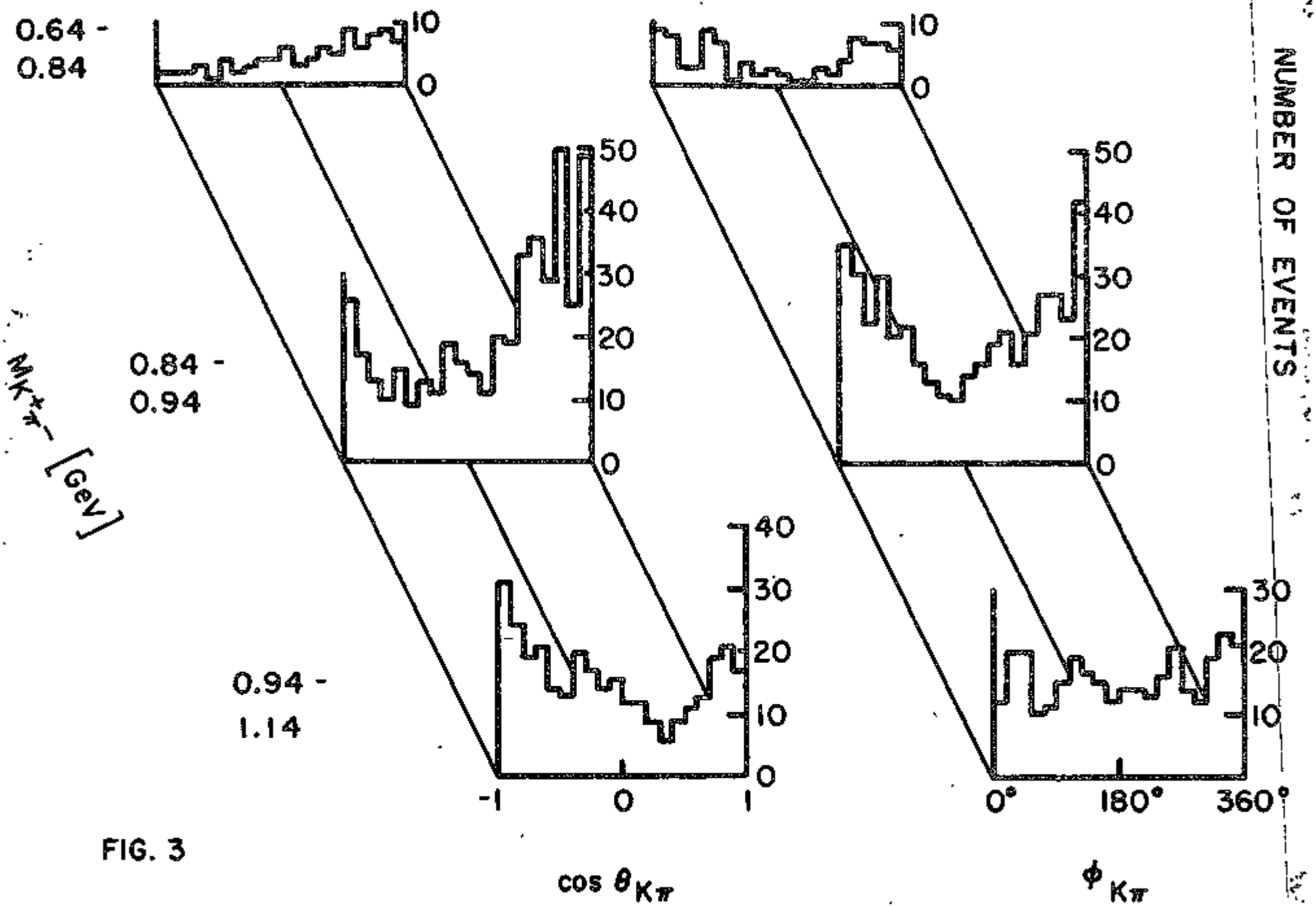
0.64 - 0.84
0.84 - 0.94
0.94 - 1.14
$M_{K^+\pi^-}$ [GeV]
NUMBER OF EVENTS
cos $\theta_{K\pi}$
$\phi_{K\pi}$
-1
0
1
0°
180°
360°

FIG. 3